

Segmenting Reddish lesions in Capsule Endoscopy Images Using a GastroIntestinal Color Space

Hai Vu*, Tomio Echigo[†], Yuma Imura[‡], Yukiko Yanagawa^{¶‡}, Yasushi Yagi[‡],

*International Research Institute MICA, Hanoi University of Science and Technology

[†]Dept. of Engineering Informatics, Osaka Electro-Communication University

[‡]The Institute of Scientific and Industrial Research, Osaka University

[¶]Technology Development Center, OMRON Corporation

Abstract—Segmenting reddish lesions in capsule endoscopy (CE) images is an initial step for further computer-assisted applications such as image enhancement, abnormal measurement/tracking, and so on. In this paper, we propose an automatic segmentation method that is successful even with CE image including unclear reddish lesions. To obtain this, the proposed method seeks good features to discriminate the reddish lesions from normal tissues. For implementations, we first extract only meaningful regions in a CE image through a pre-segmentation step. The proposed features then are extracted for the meaningful regions in stead of the whole image. We approaches segmentation task through considering a statistical operator for the extracted features, that is local mean image. Candidates of the abnormal regions are located in the local mean image with assistants of a diffusion process. Evaluations in the experiments confirm effectiveness of the proposed method with both qualitative and quantitative measurement.

I. INTRODUCTION

The capsule endoscopy (CE) technology [1] has been widely used in examining diseases in the GastroIntestinal (GI) tract. It is especially successful for finding obscure bleeding regions in the small bowel, that is difficult for the conventional endoscopy techniques [2], [3]. An obscure bleeding abnormality usually presents a color tone with more red (or reddish) than normal regions. In general term, we name these appearances as reddish lesions. The reddish lesions in CE images infer symptoms of different abnormality: bleeding, angioectasia, and erythema diseases [2], [4]. Examining characteristics of these blood-based abnormalities¹ therefore usually takes account extremely concentrations of the examining doctors. Fig. 1 shows several examples of reddish lesions in CE images. While appearance of reddish lesions in Fig. 1(a)-(b) are dominant from normal tissues, reddish lesions in Fig. 1(c)-(d) are more ambiguous and unclear. Intuitively, examining doctors need assistant tools for enhancing the image display. Segmenting the reddish lesions is an initial step for such tools. It also has important roles in evaluating abnormal types, abnormal measurements and classifications.

Regarding computer-aided tools for CE images, various state-of-the-art techniques are listed in recent surveys of Karargyris et al. [5] and Chen et al. [6]. For segmenting bleeding regions task, color and its derivations usually are favor features. Lau et al. [7] proposed a technique utilizing two-level threshold for image luminance and color saturation features. The work

¹In this paper, description about blood-based abnormalities is concerned to reddish lesions.

by Karargyris in [4] utilized features in Ohta color space [8]. Penna et al. in [9] discriminated bleeding lesions from normal regions by using Reed-Xiaoli (RX) detector [10]. For detecting bleeding regions, Giritharan et al. [11] extracts dominant color descriptor [12], which is one of MPEG-7 visual descriptors, and co-occurrence of the dominant colors. Pan et al. [13] deploys a probabilistic neural network using six color components (R,G,B,H,S,V). However, specific characteristics of the GI wall's appearance, which often distinct from other type of images, are not carefully considered. The previous works utilize color features in a full range of a color space (e.g. original RGB space or transformed space as HSV, Lab). The fact that the color tones of GI wall regions distribute quite strictly in a subspace: e.g., the stomach contains pinkish colors, while the small intestine contains pinkish-yellowish colors. To adapt with this observation, a specific color space, named GI color space, was proposed in our previous work [14]. Advantages of the GI color space is that it suggests available color ranges that definitely define to the CE images. These characteristics are useful for presenting image data of CE images, but also for discriminating abnormalities from normal tissues.

In this work, we tackle this observation suggests valuable features by evaluating discriminations between abnormal and normal regions through a training dataset in the learning procedure. The results show that discriminant characteristic is a 1-D feature that is extracted in the GI color space. It is as good discriminant as original color features (RGB triple). Based on this feature, a segmentation algorithm is proposed. A pre-segmentation step is implemented to eliminate non-wall GI regions. The image data of the meaningful regions is projected into the GI color space. After extracting the image features, a statistical version of the transformed image is calculated, that is local mean image. This operator formulates an local mean image from neighborhood regions through a sampling function at a certain scale. Candidates of the abnormal regions are located in the local mean image through a diffusion process. The experiments evaluate the bleeding segmentations with a large testing data set in term of both qualitative and quantitative measurements.

II. LEARNING FEATURES FOR DISCRIMINATING (AB)NORMALITIES

A. The feature extractions

Because GastroIntestinal (GI) color space [14] associates us in regarding works, we shortly introduce its establishment

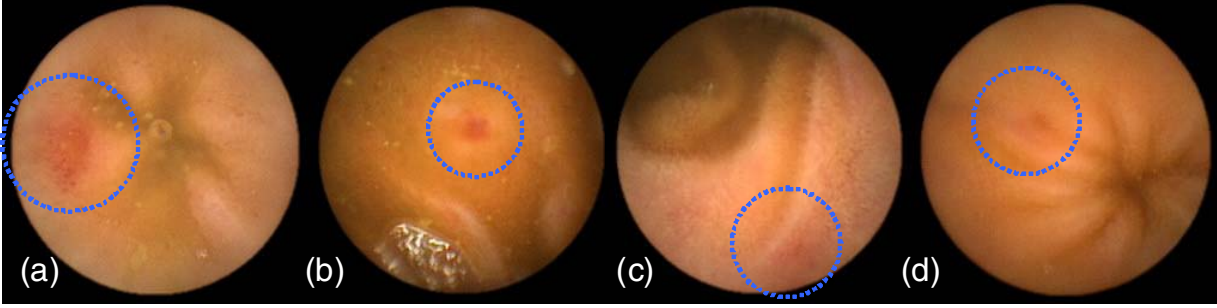


Fig. 1. Some examples of reddish lesions. (a)-(b) are clear images, whereas (c)-(d) are unclear images. Blue circles are marked around reddish lesions by examining doctors.

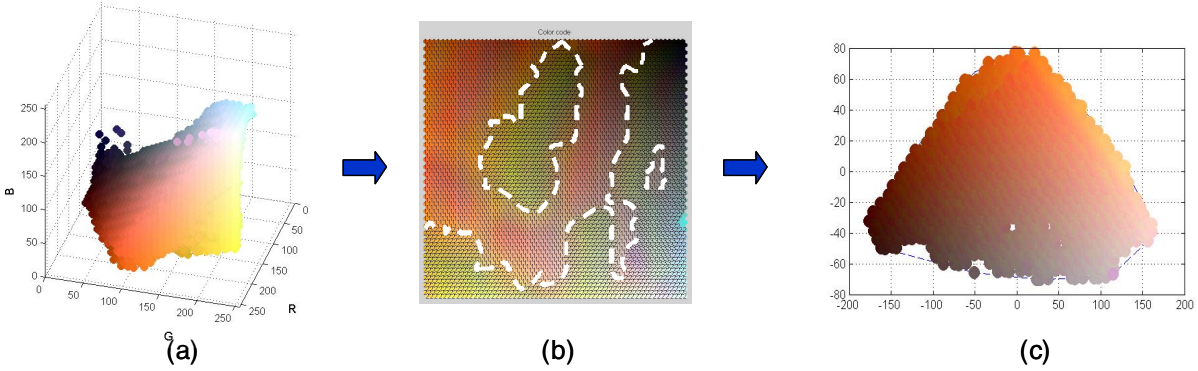


Fig. 2. The proposed GI Color space. (a) Distribution of RGB data from a large CE images. (b) Clustering color components into wall/non-wall groups. (c). Distribution of wall color components presented by two principal components (using PCA)

and features in the following section. A GI color space is constructed from a large dataset of the CE images. The most popular color components are extracted from such dataset. Fig. 2(a) plots them in the original RGB color space. As shown in Fig. 2(b), the color components of GI wall regions are located within white boundary regions of a map created by Self-Organized Map (SOM). A set of these color components is denoted as a set of Θ . The statistical characteristics of Θ also are measured through two features: eigenvectors ν_{Θ} and mean values μ_{Θ} . Hence, given a c_{rgb} color, it can be projected into the proposed GI color space following a form of PCA transformation ζ as follow:

$$c_{rgb} \rightarrow c_{pc1,pc2,pc3} : \nu_{\Theta}^T(c_{rgb} - \mu_{\Theta}) \quad (1)$$

It notes that we transform only color components of the wall regions in CE images. Therefore, a pre-segmentation step is proposed to eliminate non-wall regions from an original image. It is a quite straightforward process. First, an image is divided into blocks or windows. Size of each window region is $W \times H$. In each window, we look for pixels, whose image data belongs to a color component of Θ . Such window is considered as a wall region if total number of the pixels found larger than a threshold value. In our implementation, the threshold value is equal 70% of the window size. Then a 2-D dilation operator is applied to smoothly connect the wall regions together. Fig. 3(a)-(d) shows some examples with boundary of the wall regions. While darkness of lumen regions are eliminated in Fig. 3(a) and (d), current approach also success in cases including noises such as fluid, food, as shown in Fig. 3(b) and (c).

To learn characteristics of the reddish lesions and discriminating features, we prepare a training dataset including three common types of blooded-based pathology:

- Erythema: 134 images;
- Angiodysplasia: 64 images;
- Bleeding: 143 images;

The data set is collected from 300 patient sequences within two years in Graduate School of Medicine, Osaka City University. Reddish lesions are carefully marked by experts. Some of them with marked regions are shown in Fig. 4(a). For discriminant analysis, color features are extracted from these training dataset. Besides r, g, b channel and rgb triplet, the image features extracted in the GI color space are examined.

A triplet color components in the GI color space (pc_1, pc_2, pc_3) presents uncorrelated variables as good as possible. Furthermore, while the main components pc_1, pc_2 present commons or general appearance of wall regions, the last component pc_3 is more sensitive, especially, with small changes in neighborhood regions. This feature (pc_3) therefore is expected to well discriminate abnormal and normal regions, especially, in case of unclear reddish lesions. Finally, five features (r, g, b, rgb and pc_3 components) are extracted. We assess performance of these features using Linear Discriminant Analysis (LDA). In the empirical study below, we confirm that pc_3 component is an optimal feature. The fact that pc_3 is also more sensitive with noise data than other components.

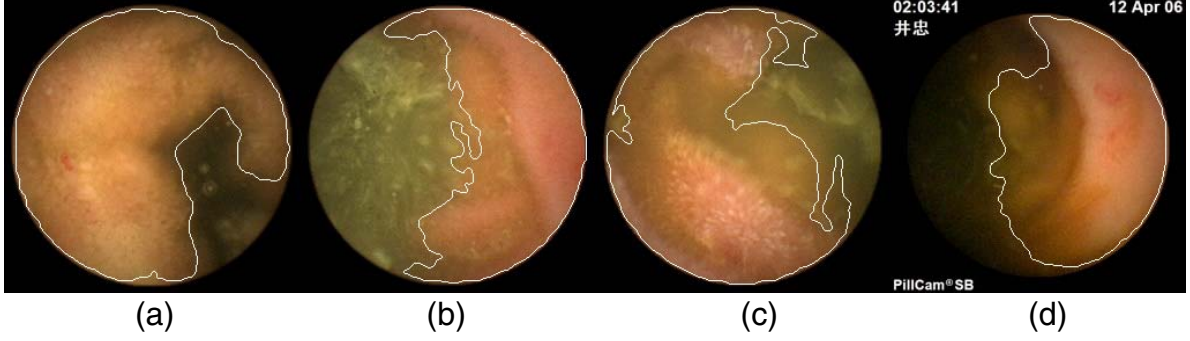


Fig. 3. (a)-(d). Results of the pre-segmentation step. Wall regions are extracted from original images

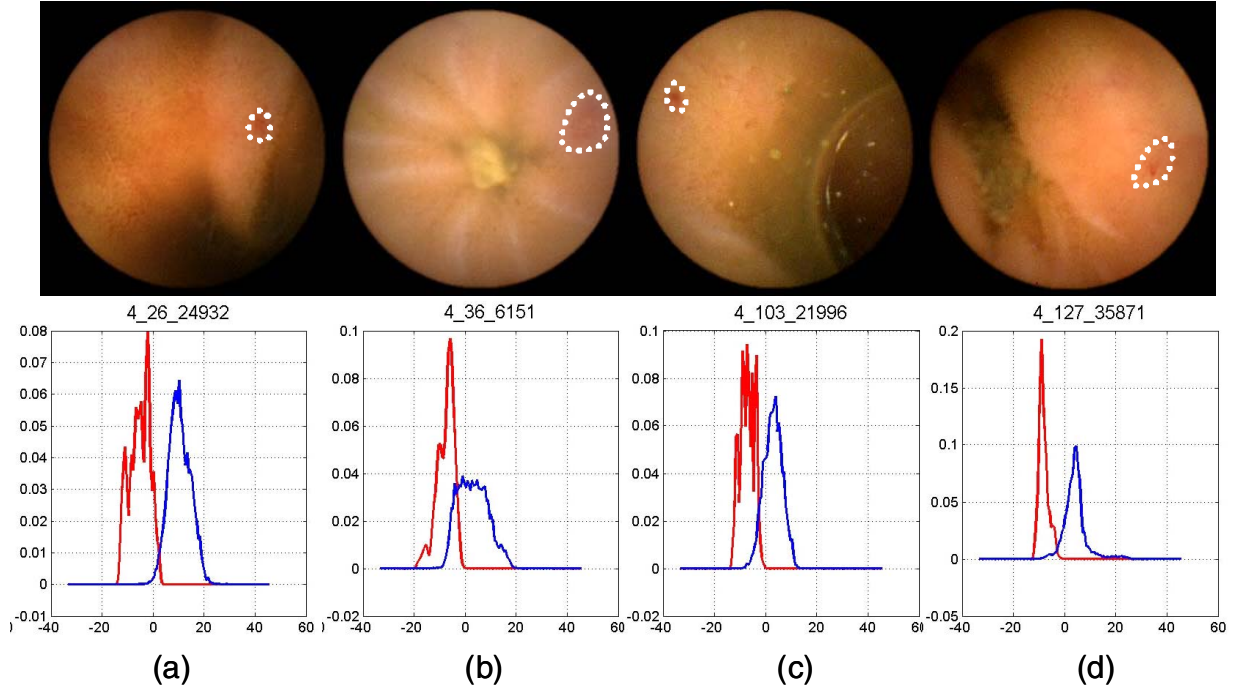


Fig. 4. (a-d) Top row is original images, the dotted lines mark boundary of abnormal regions. Bottom row is PC3 distributions of normal (blue line) and abnormal regions (red line)

However, in our segmentation scheme, only wall regions are considered, influence of noise data therefore are reduced.

B. Evaluating the features for discriminating (ab)normalities

In this empirical study, features of abnormal regions and normal regions are represented through probability density functions (PDFs). To evaluate performance of each feature, statistical classification approaches are utilized through checking pattern similarity relative between prototypes. Three distance classifiers are selected as below:

- C_1 - Minimum distance classifier (or template matching classification) based on Euclidian
- C_2 - Mahalanobis linear discriminant
- C_3 - Fisher Linear Discriminant

These classifiers are introduced in recognition textbooks, e.g Ch. 4 in [15]. Let us denote a certain feature vector as x

(with any d -dimension). Objective of a classifier C_i ($i = 1, 2, 3$) is to decide a data x as a pixel in normal region or abnormal region through a distance function d . Given a training image, each pixel belonging abnormal (w_1) or normal regions (w_2) will be checked using classifier C_i . We then evaluate its performance using a measurement of corrected rate, denoted as $corRate$. The $corRate$ of a classifier is calculated by:

$$\begin{aligned}
 corRate_1 &= \frac{\sum_{i \in w_1} t}{\sum_{i \in w_1} 1} \times 100\% \text{ with } \begin{cases} t = 1 \text{ if } d_1 < d_2 \\ t = 0 \text{ otherwise} \end{cases} \\
 corRate_2 &= \frac{\sum_{i \in w_2} t}{\sum_{i \in w_2} 1} \times 100\% \text{ with } \begin{cases} t = 1 \text{ if } d_2 < d_1 \\ t = 0 \text{ otherwise} \end{cases} \\
 corRate &= \frac{corRate_1 + corRate_2}{2}
 \end{aligned} \tag{2}$$

Average results of the $corRate$ is shown in Table I. The $pc3$ and rgb triplet features are outperform single channel (r,g,b) in all classifiers. Performance of $pc3$ and rgb triplet is also similar C_2, C_3 where correlation between variables is taken

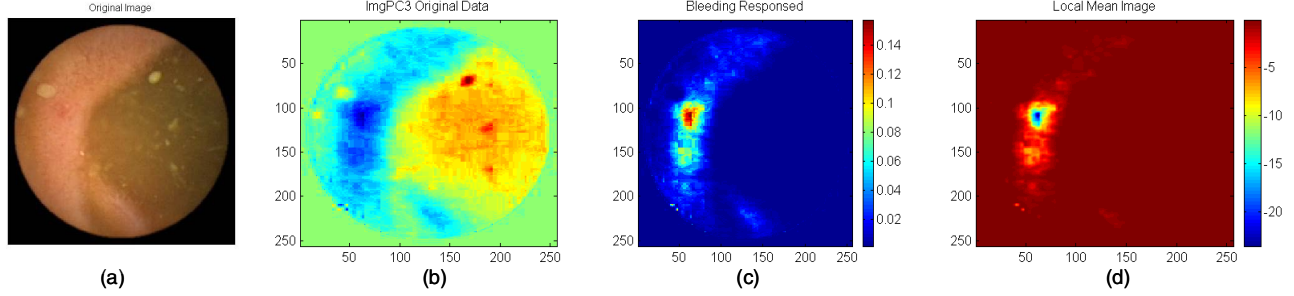


Fig. 5. Local Mean Image calculation. (a) Original Image. (b) PC3 image data. (c) Responsibility of a Gaussian ($G(50,2.5)$), (d) Local Mean Image Result

account. The results confirm that *pc3* feature presents very well discriminations between normal and abnormal regions. Fig. 4(b) shows intuitively performance of *pc3*, whose the abnormal distributions (in red lines) is obviously separated from the normal ones (in blue lines).

TABLE I. AVERAGE OF THE *corRate* WITH DIFFERENT CLASSIFIERS

Classifier	R	G	B	RGB	PC3
C_1	74	62	65.5	80.3	90.5
C_2	74	62	65.5	91.5	90.5
C_3	74	62	65.5	92.5	90.5

III. SEGMENTATION ALGORITHMS

In our proposed method, the segmentation task is approached in view of analysis of multiscale image statistics. Originally, there is an adaption between statistical analysis and image scale space. For example, multiscale image statistics in works of Yoo et al [16] seeks crucial scale through the statistical operators, image can be segmented at "natural" boundary of normal and abnormal regions without requirements of a prior knowledge (e.g, boundary, or shape of objects). In other words, the segmentation algorithms are based on estimating central moments of the probability distribution of intensities at arbitrary locations within an image across a continuously varying range of the scale.

In light of these considerations, we utilize a basic statistical operator, that is local mean image. Let consider an area of an observed image $\tilde{I}(x)$. Its values may be sampled over a local neighborhood about a particular location x using a weighting function, $h(x)$, and a convolution operator: $\tilde{I}(x) \otimes h(x)$. With respect to invariant spatial translation and rotation, the $h(x)$ function can be a normalized Gaussian function. At each scale s of the Gaussian, the statistical operator comprises of a sum of the original image intensities weighted by a Gaussian sampling kernel. With the desired s , abnormal regions in $\tilde{I}(x)$ is extractable.

A. Local mean image calculation

Utilizing the optimal feature within the meaningful region w_0 , definition of $\tilde{I}(x)$ is:

$$\tilde{I}(x) = \begin{cases} pc_3(x) & \text{if } x \in w_0 \\ 0 & \text{otherwise} \end{cases} \quad (3)$$

A normalized gaussian kernel $h(x)$ is defined at scale s by:

$$h(x) = G(x, s) = \frac{1}{\sqrt{2\pi s^2}} e^{-\frac{x^2}{2s^2}} \quad (4)$$

Where parameter s is standard derivation or spread parameter. A statistical operator such as the local mean image, denoted by $\mu(\tilde{I}(x), s)$, is defined by:

$$\mu(\tilde{I}(x), s) = E(\tilde{I}(x), s) = \sum_{x \in \omega} (G(\tilde{I}(x))\tilde{I}(x)) \quad (5)$$

Parameter ω presents a window region with size of $w \times h$ pixels (e.g, 3×3 pixels in our implementations). Fig. 5 shows a local mean image calculated using (5). In this example, the reddish lesions in the original image (Fig. 5(a)) is unclear and ambiguous. The extracted meaningful regions obviously remove contaminations. Using *pc3* data as shown in Fig. 5(b), it is more clear to discriminate abnormal and normal regions. By using a reasonable scale s , Fig. 5(c) shows probability values of the $\tilde{I}(x)$ values. Finally, Fig. 5(d) measured the abnormal regions at the desired scale s . As shown in Fig. 5(d), the abnormal regions can be intuitively located through a local peak detections. A diffusion technique is applied to the local mean image for this task.

B. Detecting local peaks by diffusion techniques

A diffusion processing is adopted to apply to the local mean image $\mu(\tilde{I}(x), s_i)$ for detecting local peaks. A desirable characteristic of a nonlinear diffusion filter is that it will encourage intra-region smoothing, while inhibit inter-region smoothing. The nonlinear diffusion technique is first introduced by Perona and Malik in [17]. Fig. 6(a) shows diffused results from the local mean image in Fig. 5(d). The desirable characteristic of the diffused image is that abnormal region is smoothed whereas it even enhances the edge with normal one.

Identifying the boundaries between abnormal and normal regions from the diffused image is a straightforward procedures. We deploy a scheme including two threshold-level. The first threshold T_1 defines a level that is a saddle level. The second threshold T_2 defines a minimum/maximum level in order to confirm actual peaks are existing within an abnormal region. The diffused image normalizes the original data into l levels ($l=64$, in our implementation). Visually, seeking threshold T_1 is similar to find pixels coded in yellow color in Fig. 6(a). T_1 value is average data as such pixels. T_2 level is a relative value between T_1 and minimum value of the diffused image. In our implementation, T_2 is equal 75% of T_1 , as shown in Fig. 6(b). By comparing the diffused image with with T_1 and T_2 , the abnormal regions is extracted, as shown in Fig. 6(c). Fig. 6(d) shows the corresponding boundary between the abnormal and normal regions in the original image.

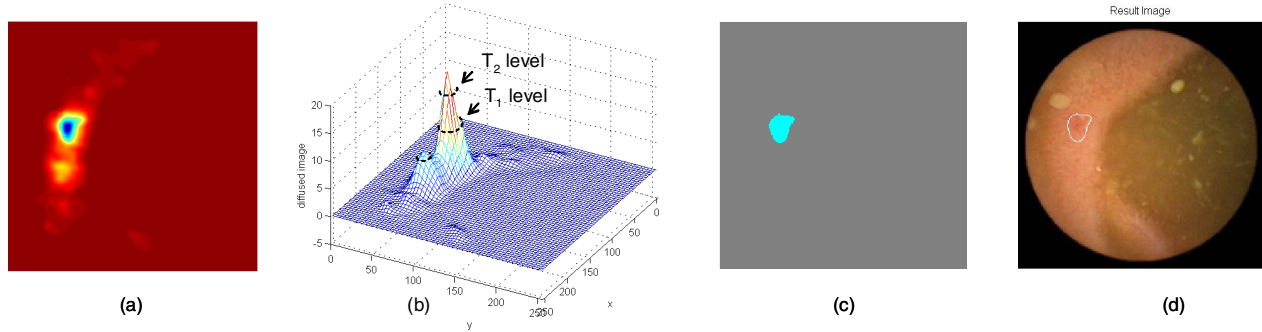


Fig. 6. Two level threshold value approach. (a) The diffused image of Fig. 5(d). (b) Two level threshold identifies local peaks. (c). A region satisfy both T_1 and T_2 thresholds (c). Boundary of abnormal region is plotted in the original image. (Fig. 5(a))

IV. EXPERIMENTAL RESULTS

For visualizing comparisons, we evaluate boundary of the proposed method with segmentation results using watershed transformation with user iterations. With a good initial scheme, segmenting abnormalities can obtain well results by the watershed algorithms (Ch. 5 in [18]). We uses an initial scheme with two markers: external and internal markers. An external marker coarsely marks boundary in order to quickly separate the abnormal regions from normal regions. Internal markers point out seed (a center area) of abnormal regions. Fig. 7 shows an example with a zoom-in version around the segmented regions. As shown, there is not so large differences between two results, even the boundary of the proposed method is more precisely. Additional segmented results are shown in Fig.8. For CE images including the scattered reddish lesions (the last row in Fig. 8), the watershed results make misunderstand with several initial markers. By using our method, the problem of segmenting scattered reddish regions is solved.

We examine quantitative measurement of the segmentation results by using two testing data. *Testset1* includes 100 images with only reddish lesions. Because they may appear in different type of abnormal regions, *Testset2* is same number of images with any type of abnormal regions (such as tumor, ulcer, polyps, so on). The ground-truth data is manually marked by circles or arrows yielded directly in diagnostic procedures of the medical experts. Segmentation results of two testing data are measured following criteria below:

- v_d the probability of detection. For a good segmentation, v_d should be close to 100%.
- v_{far} the probability of false alarm or over segmentation rate, For a good segmentation, v_{far} should be close to 0%.
- v_{un} the probability of under segmentation, i.e., the percentage of ground truth data that are not including in automatic segmentation results.

TABLE II. EVALUATION RESULTS

TestingData	v_d	v_{far}	v_{un}
<i>Testset1</i>	95	8	14
<i>Testset2</i>	90	12	29
Avg.	92	10	16

The v_d value in Table II confirms effectiveness of the proposed method. We obtain very good results for the CE im-

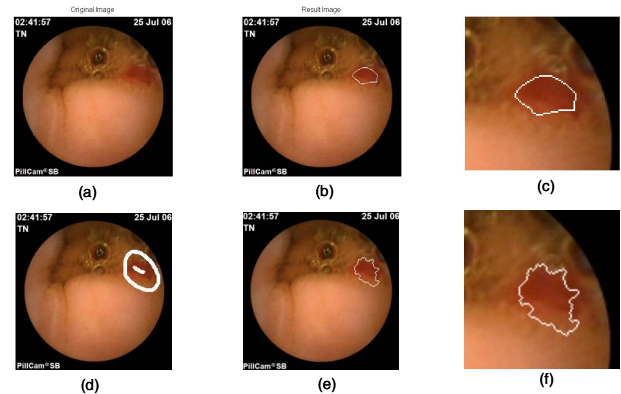


Fig. 7. Qualitative evaluation of the segmentation results. Upper row: (a) Original image. (b) The segmented abnormal regions by the proposed method. (c) A zoom-in to region around abnormal region in (b). Boundary is marked in white-line Lower row: (d) Internal and external marker are marked for applying the watershed algorithms. (e) The segmented result. (f) A zoom-in to region around abnormal region in (e)

age including reddish lesions. By using the proposed method, the segmentation results based on *Testset1* is outperform *Testset2* testing dataset, particularly for v_{un} values. The main reasons is that *Testset2* data includes different type of abnormal regions. However, the over-segmentation rate v_{far} is still quite high because the scheme to select two-level threshold value in Sec.III-B is not strong enough to eliminate noise data in local mean images.

V. CONCLUSION

This paper proposed an automatic method for segmenting the reddish lesions from CE images. The segmentation task solved problems of unclear reddish regions. We first utilized a good feature in the dedicated color space of CE images for discriminating reddish lesions from normal regions. The segmenting algorithms had impacts from the statistical image techniques. The segmentation results suffered from the experimental evaluations in both qualitative and quantitative measurements. The current segmentation results fit to applications such as image enhancement, in which the over-segmentation rate is not strictly required. In the future, a robust classification scheme can be applied to the current results to eliminate non-abnormal regions. It is expected to reduce the over-segmentation rate.

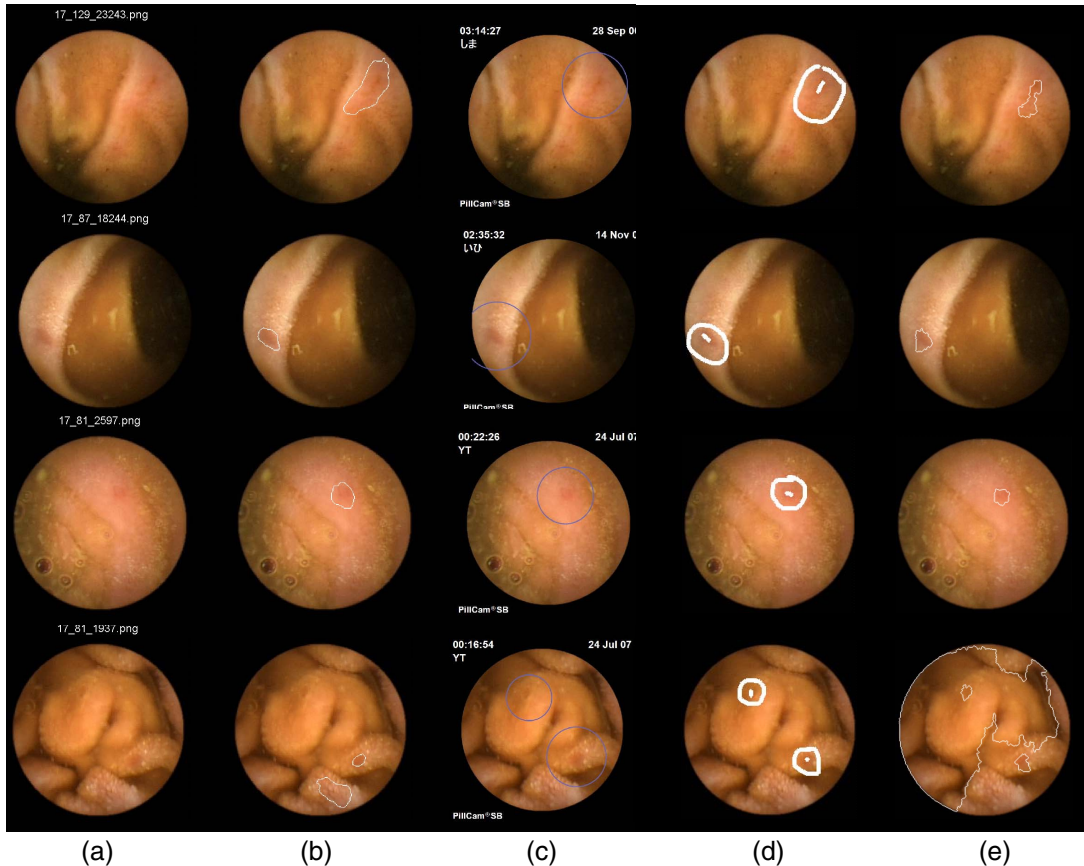


Fig. 8. Some examples of the segmentation results. In each row : (a) Original Image. (b) Segmentation results by the proposed method. (c) Ground-truth data marked by the examining doctors in blue circles. (d). Internal/External markers (manually) for watershed algorithm. (e). Watershed algorithm results

VI. ACKNOWLEDGEMENTS

The first author thanks to Vietnam National Foundation for Science and Technology Development (NAFOSTED) for their supports to fulfill the study.

REFERENCES

- [1] G. Iddan, G. Meron, A. Glukovsky, and P. Swain, "Wireless capsule endoscope," *Nature*, vol. 405, p. 417, 2000.
- [2] B. Lewis, R. Franchis, and G. Gay, "Consensus report," in *Proceeding of the 5th International Conference on Capsule Endoscopy*, 2006.
- [3] P. Swain, "Wireless capsule endoscopy," *GUT*, vol. 52, pp. 48–50, 2003.
- [4] A. KARARGYRIS, "A novel synergistic diagnosis methodology for identifying abnormalities in wireless capsule endoscopy videos," *Ph.D. Thesis - Wright State University*, 2010.
- [5] A. Karargyris and N. Bourbakis, "Wireless capsule endoscopy and endoscopic imaging: A survey on various methodologies presented," *IEEE Engineering in medicine and biology magazine*, vol. 29, pp. 72–83, Feb. 2010.
- [6] Y. Chen and J. Lee, "A review of machine-vision-based analysis of wireless capsule endoscopy video," *Diagnostic and Therapeutic Endoscopy*, vol. 2012, pp. 1–9, 2012.
- [7] P. Lau and P. L. Correia, "Detection of bleeding patterns in wce video using multiple features," in *Proceedings of the 29th IEEE International Conference on EMBS*, Aug 2007, pp. 5601–5604.
- [8] T. K. Y. Ohta and T. Sakai, "Color information for region segmentation," *Computer Graphics and Image Processing*, vol. 13, pp. 222–241.
- [9] B. Penna, T. Tilloy, and M. Grangetto, "A technique for blood detection in wireless capsule endoscopy images," in *Proceedings of the 17th European Signal Processing Conference*, Aug 2009, pp. 1864 – 1868.
- [10] I. Reed and X. Yu, "Adaptive multiband far detection of an optical pattern with unknown spectral distribution," *IEEE Trans. on Acoustics, Speech and Signal Processing*, vol. 38, no. 10, pp. 1760–1770, Oct 1990.
- [11] B. Giritharan, X. Yuan, and J. Liu, "Bleeding detection from capsule endoscopy videos," in *Proceedings of the 30th IEEE International Conference on EMBS*, 2008, pp. 4780 – 4783.
- [12] V. V. B.S. Manjunath, J.-R. Ohm and A. Yamada, "Color and texture descriptors," *IEEE Transactions on Circuits and Systems for Video Technology*, vol. 11, no. 6, pp. 703–715, Jun. 2001.
- [13] G. Pan, G. Yan, X. Qiu, and J. Cui, "Bleeding detection in wireless capsule endoscopy based on probabilistic neural network," *Journal of Medical System*, pp. 1–8, 2010, 10.1007/s10916-009-9424-0.
- [14] H. Vu, T. Echigo, K. Yagi, M. Shiba, K. Higuchi, T. Arakawa, and Y. Yagi, "Color analysis for segmenting digestive organs in vce," in *Proceeding of 20th International Conference on Pattern Recognition*, Aug., pp. 2468 – 2471.
- [15] J. de Sa', *Pattern Recognition - Concepts, Methods and Applications*. Springer-Verlag, 2001.
- [16] T. Yoo, "Scale and statistics in variable conductance diffusion," in *Proceedings of the AAAI Symposium on Applications of Computer Vision in Medical Image*, Mar. 1994.
- [17] P. Perona and J. Malik, "Scale-space and edge detection using anisotropic diffusion," *IEEE Trans. on PAMI*, vol. 12, pp. 629–639, Jul. 1990.
- [18] A. Bovik, *Handbook of Image and Video Processing*. ACADEMIC PRESS, 2000.